2D Time-frequency interference modelling using stochastic geometry for performance evaluation in Low-Power Wide-Area Networks

Zhuocheng Li*,†, Steeve Zozor*, Jean-Marc Brossier*, Nadège Varsier† and Quentin Lampin†
* Univ. Grenoble Alpes, GIPSA-Lab, F-38000 Grenoble, France
Emails: (zhuocheng.li,steeve.zozor,jean-marc.brossier)@gipsa-lab.grenoble-inp.fr
† Orange Labs, Meylan, France, Emails: (zhuocheng1.li,quentin.lampin,nadege.varsier)@orange.com

***Abstract*—In wireless networks, interferences between transmissions are modelled either in time or frequency domain. In this article, we jointly analyze interferences in the time-frequency domain using a stochastic geometry model assuming the total time-frequency resources to be a two-dimensional plane and transmissions from Internet of Things (IoT) devices time-frequency patterns on this plane. To evaluate the interference, we quantify the overlap between the information packets: provided that the overlap is not too strong, the packets are not necessarily lost due to capture effect. This flexible model can be used for multiple medium access scenarios and is especially adapted to the random time-frequency access schemes used in Low-Power Wide-Area Networks (LPWANs). By characterizing the outage probability and throughput, our approach permits to evaluate the performance of two representative LPWA technologies Sigfox® and LoRaWAN®.**

***Index Terms*—2D time-frequency interference; time-frequency random access; capture effect; stochastic geometry; IoT; LPWANs.**

I. Introduction

Trading bit rates for better link budgets, LPWANs provide long range wireless connectivity to IoT devices [1], [2], [3]. Such networks provide a promising alternative to traditional cellular or multi-hop networks and are indeed envisioned to provide nationwide connectivity over industrial, scientific and medical (ISM) bands to battery-powered IoT devices that transmit little amount of data over long periods of time, *e.g.,* water & gas meters. Thanks to the long range, the IoT devices can communicate directly with the base stations in a star topology.

Random access schemes such as Aloha are commonly used in LPWANs in which multiple devices access frequency resources with neither carrier sensing nor contention mechanisms [4], [5]. This reduces the communication overhead and the packet air time, but it increases the risk of collisions between packets when they overlap in time domain. Multiple works have been dedicated to the interferences modelling in time domain [6], [7], [8], [9]. In [8], the product of power and overlapping time duration between a transmission of interest and an interfering transmission is used to represent the quantity of interfering, then the sum is taken over multiple interfering transmissions to give the total interference.

Note that interference modelling of transmission overlapping in frequency domain is also well studied in the partially overlapped channels (POC) scenarios [10], [11], [12], which are commonly used for networks such as IEEE 802.11. The interference factor in the case of POC is evaluated as the accumulated energy in overlapped frequency domain [10]. It has been proven that the use of POC can indeed improve the network throughput in comparison to common orthogonal channelization schemes [12], [10].

Our work differs from the aforementioned interference models in that it's the first, to the best of our knowledge, to consider the joint overlapping in both time and frequency domains. Our model based on stochastic geometry is a high-level flexible one which can be adapted to multiple scenarios.

In section II, existing works on LPWANs performance evaluation are introduced. In section III, our interference modelling approach is described and expressions of SINR, outage probability and network throughput are given. Then in section IV, we give the results on probabilistic evaluation of overlapping. Finally in section V, the developed model is used to study performances of two different LPWA technologies, Sigfox® and LoRaWAN®. Section VI concludes the article and introduces some research perspectives.

II. Related Work

Multiple works exist for the performance evaluation of LPWANs [13], [14], [15], [16]. Most of these works use Poisson processes to model the packet arrival, which we believe is not the most adapted for periodic packet sending scenarios in LPWANs. For example, a device reporting on a daily basis would not send more than one message per day. However, as Poisson models the intensity of packet arrival, an intensity of one message per day represents in fact the mean value, *i.e.*, one message on average per day, which is not quite the case described. In [13], multiple annuli LoRaWAN® cell structure is well modelled and illustrated with a few applicative scenarios. This structure is considered in our article but channel effects and capture effect are added to our model thus making it more complete and realistic. In [14], the performances of a random Frequency Division Multiple Access (random FDMA) scenario are studied in the pure Aloha case, but the capture effect with little overlap between packets is not considered. In [16], the performances in terms of packet delivery ratio and throughput of LoRaWAN®

and Sigfox® are simulated. However, the simulation process and the numerous network parameters are not exposed enough thus lacking of transparency and possibility of reuse. In [15], some interesting insights on the limits of LoRaWAN® are given, but again the model is based on Poisson process and there is no possible extension to account for the capture effect. In this article, in order to give the limit of the performance, we study the outage probability and throughput of LoRaWAN® and Sigfox® when every node is transmitting as frequently as possible, according to either the ISM band duty cycle constraints or technology-related constraints, which result in message sending periods in the order of 1 to 10 minutes. This scenario of the saturation throughput could be that of packet and object tracking systems [17]. Other less frequent IoT scenarios such as water & gas metering can be evaluated using our model thanks to its flexibility.

III. The "cards tossing" model

A. Assumptions

N devices I_k share limited time-frequency resources denoted by $[0\,;\,T] \times [0\,;\,F]$ to send packets to a single base station, with $k = 0, 1 \dots N-1$. F is the bandwidth and T the message sending period. I_0 is the user of interest. $g_k(t,f)$ the packet sent by user I_k. We make the following assumptions:

1) Messages from all the senders have the same rectangle-shaped time-frequency support, since they are limited in time duration, denoted by Δt and bandwidth occupancy, denoted by Δf. Then g_k takes the form $g_k(t,f) = m_k(t,f)\,\mathbb{1}_{I_k}(t,f)$ where $\mathbb{1}_A$ stands for the indicator function of set A and $I_k = [t_k\,;\,t_k+\Delta t] \times [f_k\,;\,f_k+\Delta f]$ denotes the time-frequency support of node I_k (for the sake of simplicity, we use the same notation I_k for the sender itself and the time-frequency support of its message); t_k is the initial time of transmission and f_k the lowest frequency of the packet. $t_k \in [0; T-\Delta t]$, and $f_k \in [0; F-\Delta f]$ (see figure 1).
2) There is no cooperation between the devices, *i.e.,* random access considered. The couples (t_k, f_k) are thus independent. They are also assumed to be uniformly distributed, as it is probably optimal in terms of dispersing the packets and avoiding collisions.
3) Given support I_k, the time-frequency energy of the information packet is uniformly distributed over I_k, *i.e.,* $\mathbb{E}\left[|g_k(t,f)|^2 \,|\, I_k\right] = \rho_k \mathbb{1}_{I_k}(t,f)$, where ρ_k is the energy density.
4) The channel is affected by an additive time-frequency white noise $\xi(t,f)$ of energy density γ, *i.e.,* $\mathbb{E}\left[|\xi(t,f)|^2\right] = \gamma$.

Assumption 3 is the ideal and most efficient way of using time-frequency resources [10]. In practice, transmit spectrum mask is usually applied to specify the upper limit of power permissible and attenuate the signal outside the mask. An attenuation of 30dB to 50dB is observed in real-world scenarios [10], so this assumption can be considered as realistic. Notice that the common Aloha scenario is encompassed in this formalism by fixing $\Delta f = F$. In this case, $f_k = 0$ but t_k remains random.

B. SINR *expression*

As mentioned in the introduction, interference can be modelled as the sum of accumulated energy in time-frequency domain, which is calculated as the sum of energy coming from different interfering transmissions. The SINR is defined as the ratio between the energy of the message of interest, $\int_{I_0} \mathbb{E}\left[|g_0(t,f)|^2\right] \mathrm{d}t\,\mathrm{d}f$ and the interference $\sum_{k=1}^{N-1} \int_{I_0 \cap I_k} \mathbb{E}\left[|g_k(t,f)|^2\right] \mathrm{d}t\,\mathrm{d}f$ plus noise, *i.e.,*

$$\mathrm{SINR} = \frac{\rho_0\,\Delta t\,\Delta f}{\sum_{k=1}^{N-1} \rho_k\,S_k + \gamma\,\Delta t\,\Delta f} \tag{1}$$

where $S_k = \mu\left(I_0 \cap I_k\right)$ is the surface between the transmission of interest I_0 and an interfering one I_k (μ is the surface measure). We can normalize S_k with respect to the surface of the time-frequency support of transmissions, *i.e.*, $X_k = \frac{S_k}{\Delta t\,\Delta f}$. Thus, the SINR can be recast as

$$\mathrm{SINR} = \frac{\rho_0}{\sum_{k=1}^{N-1} \rho_k\,X_k + \gamma} \tag{2}$$

The overlapping phenomenon between packets is similar to the game of players tossing cards onto a table and trying to recognize their own cards afterwards (see figure 1). When there are too many players, the probability of overlapping will increase to the extent that it's highly probable to be unable to recognize a card. In the next subsection, we illustrate in two different scenarios, the interest of our "cards tossing" model in the derivation of the outage probability and throughput of wireless systems in function of the number of devices N.

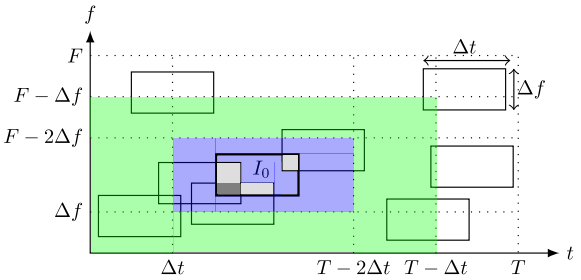

Fig. 1. Illustration of the "cards tossing" game, where each rectangle represents the information packet I_k. The rectangle in bold represents the transmission of interest, *i.e.,* the packet I_0, while the gray areas depict the sub regions in collision (the darker the area, the larger the number of "cards" covering the sub region). The light blue area is defined as the non border area $[\Delta t; T-2\Delta t] \times [\Delta f; F-2\Delta f]$, denoted by $\overline{B}$. The light green defined as the border area $[0; T-\Delta t] \times [0; F-\Delta f] \setminus \overline{B}$. These two areas constitute $[0; T-\Delta t] \times [0; F-\Delta f]$.

C. Outage and throughput model

1) With multipath fading and path loss: The first scenario is when the packets from devices suffer from path loss and fading. ρ_k can be thus expressed as $\rho_k = \rho_{tm} h\, l(r_k)$.

- ρ_{tm} models the transmission energy density, which is supposed to be identical for all devices.
- $l(r_k)$ models the distance-dependent attenuation, *e.g.,* path loss, where r_k is the Euclidean distance between device k and the base station. We choose the following non singular model [18] expressed as $l(r_k) = \alpha \left[\max(r_k, r_c)\right]^{-\beta}$, where r_c is a critical distance to avoid $l(r_k)$ taking infinity when r_k tends to 0. Here we fix it to 1m. α is a constant modelling system-level losses and gains which is fixed to 1 in our study. β is the path loss exponent assumed to be greater than 2.
- h is a random variable modelling small scale, large-scale or composite distance non dependent fading. We suppose that $\sqrt{h}$ results from a rayleigh multipath fading which gives h exponential cumulative distribution function (cdf), *i.e.*, $P_H(h) = 1 - \exp(-\lambda h)$ (with P denoting the cdf and $\mathbb{E}(h) = \lambda$). The mean value λ is fixed to 1 in our study. Note that other forms of fading can be considered with our paradigm.

The SINR can be thus recast as follows,

$$\mathrm{SINR} = \frac{h}{\frac{\sum_{k=1}^{N-1} r_k^{-\beta}\, h\, X_k}{r_0^{-\beta}} + \frac{\gamma}{\rho_{tm}\, r_0^{-\beta}}} \tag{3}$$

In order to study the distance distribution of devices in the cell, we define $r_{\max}$ as the distance to the base station of the most distant devices, in the sense that their transmissions barely satisfy the target SINR, denoted by ζ in the presence of only path loss, *i.e.*, $\frac{\rho_{tm} r_{\max}^{-\beta}}{\gamma} = \zeta$. This gives us $r_{\max} = \sqrt[\beta]{\frac{\rho_{tm}}{\zeta\gamma}}$.

Let us denote Pr the probability measure. Suppose that every packet is repeated n_{rep} times, and the repetitions are independent. The outage probability can be defined as $\left[\Pr\left[\mathrm{SINR} < \zeta\right]\right]^{n_{\mathrm{rep}}}$, which is further expressed as follows,

$$\mathrm{OP}_{n_{\mathrm{rep}}}(r_0) = \left[\Pr\left[h < \frac{r_{\max}^{-\beta}}{r_0^{-\beta}} + \frac{\zeta \sum_{k=1}^{N-1} r_k^{-\beta}\, h\, X_k}{r_0^{-\beta}}\right]\right]^{n_{\mathrm{rep}}} \tag{4}$$

Note that repetition mechanism is a commonly used scheme in LPWANs to trade efficiency for robustness of transmission.

Naturally, $\mathrm{OP}_{n_{\mathrm{rep}}}(r_0)$ depends on the position of the device of interest. Distant devices with larger r_0 suffer from greater $\mathrm{OP}_{n_{\mathrm{rep}}}(r_0)$. Suppose that the devices are uniformly distributed in the cell of the base station, which is defined as in the shape of an annulus formed with smaller radius r_c and larger radius $r_{\max}$. The probability density function (pdf) of r_k can be expressed as $p_R(r) = \frac{2r}{r_{\max}^2 - r_c^2}$ (p is used to denote the pdf). The notation k is omitted for the sake of simplicity.

Global outage probability $\overline{\mathrm{OP}}_{n_{\mathrm{rep}}}$ is defined as the outage probability averaged over r_0, *i.e.,*

$$\overline{\mathrm{OP}}_{n_{\mathrm{rep}}} = \int_{r_c}^{r_{\max}} \mathrm{OP}_{n_{\mathrm{rep}}}(r_0)\, \frac{2r_0}{r_{\max}^2 - r_c^2} dr_0 \tag{5}$$

The effective throughput is defined as the average number of non repetitive packets received per unit time and is denote by $Th(n_{\mathrm{rep}})$, which can be expressed as follows,

$$Th(n_{\mathrm{rep}}) = \frac{N(1 - \overline{\mathrm{OP}}_{n_{\mathrm{rep}}})}{T\, n_{\mathrm{rep}}} \tag{6}$$

Recall that N is the number of devices, and T the message sending period. In the case of pure Aloha, *i.e.*, packets considered lost when they collide in time or frequency domain, *i.e.*, $X_\Sigma = \sum_{k=1}^{N-1} X_k \neq 0$. Assuming X_k and r_k independent, our outage probability can be recast as,

$$\mathrm{OPAloha}_{n_{\mathrm{rep}}}(r_0) = \left[\Pr\left[X_\Sigma \neq 0\right] + \Pr\left[X_\Sigma = 0\right] \Pr\left[h < \frac{r_{\max}^{-\beta}}{r_0^{-\beta}}\right]\right]^{n_{\mathrm{rep}}} \tag{7}$$

One can observe that (7) is greater than (4), as (4) includes the capture effect, *i.e.*, certain packets not considered lost even in case of collision. $\overline{\mathrm{OPAloha}}_{n_{\mathrm{rep}}}$ and $ThAloha(n_{\mathrm{rep}})$ can be calculated in the similar way. By definition, $\overline{\mathrm{OPAloha}}_{n_{\mathrm{rep}}} \leq \overline{\mathrm{OP}}_{n_{\mathrm{rep}}}$ and $ThAloha(n_{\mathrm{rep}}) \leq Th(n_{\mathrm{rep}})$.

2) With perfect power control: We consider another scenario in which the packets of different devices are supposed to arrive at the base station with identical energy density, *i.e.*, $\rho_0 = \rho_k = \rho$, thanks to a certain power control mechanism. The SINR can be recast in this case as,

$$\mathrm{SINR} = \frac{1}{X_\Sigma + \mathrm{SNR}^{-1}} \tag{8}$$

where $\mathrm{SNR} = \frac{\rho}{\gamma}$. The outage probability can be recast as,

$$\mathrm{OP}_{n_{\mathrm{rep}}} = \left[\Pr\left[X_\Sigma \geq \zeta^{-1} - \mathrm{SNR}^{-1}\right]\right]^{n_{\mathrm{rep}}} \tag{9}$$

In this case the non fairness between devices in terms of distance to the base station is resolved. $\mathrm{OP}_{n_{\mathrm{rep}}}$ does not depend on r_0 any more, but only on γ, the target SINR ζ and ρ, the energy density that results from the power control. The average throughput can be recast as $Th(n_{\mathrm{rep}}) = \frac{N(1 - \mathrm{OP}_{n_{\mathrm{rep}}})}{T\, n_{\mathrm{rep}}}$. The quantities to be simulated are listed in table II.

In both scenarios, we should first study the probabilistic distributions of X_k and X_Σ. In the next section, we derive the probabilistic evaluations of X_k and X_Σ. In the case of multipath fading and path loss, the exact distribution of $\sum_{k=1}^{N-1} r_k^{-\beta}\, h\, X_k$ remains difficult to evaluate even with the distribution of X_k derived and r_k, h and X_k assumed to be independent random variables. We use Monte Carlo method to evaluate it.

IV. Probabilistic Evaluations

The results of X_k and X_Σ are different in 1D case and 2D case. We first give the results of X_k in the easier 1D case in section IV-A, *i.e.*, $\Delta f = F$ so interference happens only when there is overlap in time domain. Physical layer technologies such as spreading spectrum fall into this case. Then the results of X_k in the more complicated 2D case are given in section IV-B, where overlapping can happen in both time and frequency domains, random FDMA approach belongs to this case. The results on X_Σ are given in section IV-C.

We denote by p_{X_k} (resp. p_{X_Σ}) the pdf of X_k (resp.X_Σ), by P_{X_k} (resp. P_{X_Σ}) the cumulative distribution function (cdf) of X_k (resp. X_Σ).

The overlapped surface between two packets X_k is determined by their relative position in $[0;T]\times[0;F]$. Recall that t_k and f_k are defined over$[0\,;\,T-\Delta t]$ and $[0\,;\,F-\Delta f]$. We can thus define $\tau_k = \frac{|t_k - t_0|}{\Delta t}$ and $\varphi_k = \frac{|f_k - f_0|}{\Delta f}$ as the normalized absolute time and frequency difference between emission I_0 and I_k, see figure 2. τ_k and φ_k are defined over $[0\,;\,N_t-1]$ and $[0\,;\,N_f-1]$ respectively. From the assumption 2, (τ_k, φ_k) also have identical distributions. For the sake of brevity, we will omit index k in the expressions, *i.e.,* pdf of (τ_k, φ_k) (resp. τ_k and φ_k) is denoted by $p_{\tau,\varphi}$ (resp. p_τ and p_φ) , and the (cdf) denoted by $P_{\tau,\varphi}$ (resp. P_τ and P_φ).

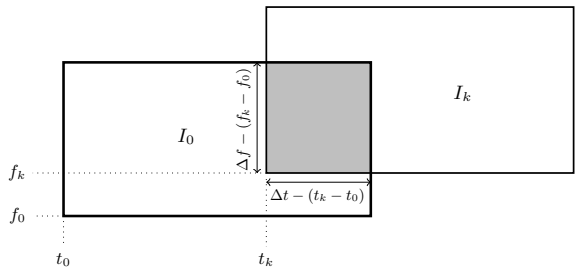

Fig. 2. When an emission I_k collides with I_0, the overlapped surface, represented in gray, is $(\Delta t - |t_k - t_0|)(\Delta f - |f_k - f_0|)$.

A. 1D "cards tossing" game

In the 1D game, $f_0 = f_k = 0$ so that $\varphi_k = 0$. f_k and φ_k become deterministic and independent of t_k. We have

$$X_k = (1-\tau_k)\mathbb{1}_{[0\,;\,1)}(\tau_k) \tag{10}$$

One can easily deduce that

$$\Pr[X_k > x] = \int_0^{1-x} p_\tau(u)du \tag{11}$$

which gives $\Pr[X_k > x] = P_\tau(1-x)$ and the probability of collision $p_c = \Pr[X_k > 0]$ is given by $P_\tau(1)$.

In the case where t_k are assumed uniformly distributed over $[0\,;\,T-\Delta t]$, the cdf of X_k, P_{X_k} can be derived as follows,

$$P_{X_k} = 1 - \Pr[X_k > x] = 1 - \frac{(2N_t - 3 + x)(1-x)}{(N_t-1)^2} \tag{12}$$

where $x \in [0\,;\,1)$. p_{X_k} can be obtained by deriving P_{X_k} for $x \neq 0$, and $p_{X_k}(0) = P_{X_k}(0) = 1 - \frac{2N_t-3}{(N_t-1)^2}$.

B. 2D "cards tossing" game

Recall that t_k and f_k are assumed independent and uniformly distributed over $[0\,;\,T-\Delta t]$ and $[0\,;\,F-\Delta f]$. Denote $\frac{T}{\Delta t}$ by N_t and $\frac{F}{\Delta f}$ by N_f.

A simple look at the geometrical configuration plotted in figure 2 allows to express the normalized surface as

$$X_k = (1-\tau_k)(1-\varphi_k)\mathbb{1}_{[0\,;\,1)^2}(\tau_k, \varphi_k) \tag{13}$$

Thus, for $x \in [0\,;\,1)$, we have $\Pr[X_k > x] = \Pr[(1-\tau_k)(1-\varphi_k) > x]$, we immediately get,

$$\Pr[X_k > x] = \int_0^{1-x} \left(\int_0^{1-\frac{x}{1-u}} p_{\tau,\varphi}(u,v)\,dv \right) du \tag{14}$$

where the bound of the first integral is due to the fact that when $u \geq 1-x$, $1 - \frac{x}{1-u} \leq 0$, the inner integral is zero. The probability of collision is $p_c = P_{\tau,\varphi}(1,1)$. When t_k and f_k are independent and uniformly distributed over $[0\,;\,T-\Delta t]$ and $[0\,;\,F-\Delta f]$, some long algebra leads to,

$$P_{X_k} = 1 - \frac{(a + b\,x)(1-x) + (c+x)x\ln x}{(N_t-1)^2(N_f-1)^2}$$

with

$$\begin{cases} a &= (2N_t - 3)(2N_f - 3) \\ b &= 9 - 2N_t - 2N_f \\ c &= 2\,(N_t - 2)(N_f - 2) \end{cases} \tag{15}$$

Similar procedures as in 1D game should be taken to find p_{X_k}.

C. Probabilistic evaluation of X_Σ

Let's first consider the probabilistic evaluation of X_Σ in the 2D case. Notice that $[0;T-\Delta t]\times[0;F-\Delta f]$ can be divided into two areas *i.e.,* the non border area denoted by $\overline{B}$ and the border area denoted by B. We have $\overline{B} = [\Delta t; T-2\Delta t] \times [\Delta f; F-2\Delta f]$, and $B = [0;T-\Delta t]\times[0;F-\Delta f]\,/\overline{B}$. See figure 1. For the sake of brevity, we define the event that (t_0, f_0) falls into the non border area $\overline{B}$ also as $\overline{B}$. The event that (t_0, f_0) falls into the border area as B.

In fact $p_{X_k|\overline{B}} \neq p_{X_k|B}$ because a packet in $\overline{B}$ has greater chance to be corrupted by an interfering one as it can come from all directions. A packet in B cannot be interfered from certain positions of (t_k, f_k) out of border, resulting in a smaller probability of being corrupted. In section IV-A and IV-B, we could have separated the derivation in $\overline{B}$ and B and obtained the same results. For P_{X_Σ}, instead of evaluating it separately in $\overline{B}$ and B, we give the approximation as follows,

$$\begin{aligned} P_{X_\Sigma} &= P_{X_\Sigma|\overline{B}} \Pr(\overline{B}) + P_{X_\Sigma|B} \Pr(B) \\ &\approx P_{X_\Sigma|\overline{B}} \\ &= P_{X_k|\overline{B}} * p^{(k-1)*}_{X_k|\overline{B}} \\ &\approx P_{X_k} * p^{(k-1)*}_{X_k} \end{aligned} \tag{16}$$

where $*$ stands for convolution, and $(k-1)*$ the $(k-1)$ times convolution. When $\Pr(\overline{B}) \gg \Pr(B)$ (This hypothesis is realistic in the case where $T \gg \Delta t$ and $F \gg \Delta f$, which is verified in most LPWANs scenarios [1], [2], [3], [13], [19], [15], [16]), the first approximation is obviously valid. The second approximation comes from $P_{X_k} = P_{X_k|\overline{B}} \Pr(\overline{B}) + P_{X_k|B} \Pr(B) \approx P_{X_k|\overline{B}}$, and it's the same with p_{X_k}. We use P_{X_k} and p_{X_k} obtained in the case of independent and uniform distribution in section IV-A and IV-B to evaluate (16).

The reasoning and the evaluation of X_Σ in the 1D case is similar and thus omitted.

V. Application

Let us now illustrate how our model can be used to evaluate the performance of two LPWA technologies.

A. *Sigfox*®

1) 2D "cards tossing" parameters: First, we consider Sigfox®, an LPWA technology based on Ultra Narrow Band (UNB) [14]. The packet takes only a bandwidth Δf around 100Hz. In doing so, the noise power $\gamma\Delta f$ is greatly reduced and the transmission range is thus increased. In the physical layer, binary phase-shift keying (BPSK) is used. In the medium access control (MAC) layer, random FDMA scheme is adopted [19], *i.e.*, due to transmitter oscillator's jitter, it's not possible to channelize, so a packet is transmitted at a randomly chosen frequency in the available frequency band of 40kHz.

Sigfox® also limits the number of messages per node to 140 messages per day, which equals to a message around every 617s [16]. T is fixed to 617s, *i.e.*, devices transmit as frequently as possible. The maximal allowed payload size per packet is 12 bytes. With the preamble and cyclic redundancy check (CRC) fields, the transmission duration Δt of a packet is around 1.76s [20]. Note that this Δt and T satisfy the European Telecommunications Standards Institute (ETSI) requirement of 1% duty cycle constraints in the 868MHz band [21]. The "cards tossing" game of Sigfox® falls into the 2D case described in IV-B and its parameters, *i.e.*, Δf, F, Δt and T are given in table I.

2) Outage and throughput model for Sigfox®: For now, there is no report of any power control mechanism in Sigfox®, so the model introduced in III-C1 is chosen. Parameters ρ_{tm}, γ, ζ, β, $r_{\max}$ are also listed in table I. The derivation of these parameters is as follows.

The maximum transmission power in 868MHz is fixed to 14dBm *i.e.*, $\rho_{tm}\Delta f = 14$dBm [21]. Thanks to UNB, Sigfox® benefits from a reduced noise floor around -154dBm, *i.e.*, $\gamma\Delta f = -154$dBm. This gives us a link budget around 168dB. Let's consider a reception threshold of 8dB, a shadow fading margin of 10dB as well as a penetration loss of around 15dB for urban environment. This gives us a target SINR around 33dB, *i.e.*, $\zeta(\text{dB}) = 33$dB. Finally let's consider a path loss exponent β of 3.6 for urban environment. All of these parameters give us a $r_{\max}$ of 5.2km for urban scenario.

3) Simulation: Taking all the parameters of Sigfox®, formulae (4)–(5)–(6)–(7) expressing the first 6 quantities listed in II (For the definition of SF, see section V-B) are simulated and the results are given in figures 3 and 4.

Figure 3 shows that capture effect represented by the difference between the solid and dashed lines decreases with the distance r_0, because naturally the devices nearer to the base station have more chances to benefit from the capture effect. Repetitions do reduce the outage probability.

Figure 4 shows that $\overline{\text{OP}}_{n_{\text{rep}}}$ is not greatly reduced in the capture case than in the pure Aloha case; the improvement in $Th(n_{\text{rep}})$ increases with N, as more collisions happen with higher N, thus amplifying the capture effect, but the high collision regime is not the optimal zone for the low-power devices to function. Device density $p_R(r)$ increases with distance r_0 and further devices barely benefit from the capture effect, so devices at the cell edge are probably the bottleneck of the network performance, *i.e.*, it's them that stops the network performance from getting better. One can also observe that repetitions reduce the global outage probability but also result in lower effective throughput because of the introduced

TABLE I
Table of Notations

	Sigfox®	LoRa®
Outage and throughput model	With path loss and fading	Perfect power control
"cards tossing" model	2D	1D
Transmission power ρ_{tm} Δf(dBm)	14	See section V-B3
Noise floor $\gamma\Delta f$(dBm)	-154	-117
Target SINR ζ (dB)	33	See table III
Path loss exponent β	3.6	3.6
Range $r_{\max}$ (km)	5.2	See table III
Cell form	Single annulus	Multiple annuli
Payload size (bytes)	12	See table III
Application bit rate (bits/s)	54.5	See table III
F(kHz)	40	125
Δf	100Hz	125kHz
T(s)	617	See table III
Δt(s)	1.76	See table III
Number of channels	1	3

TABLE II
Table of Simulated Quantities

$\text{OP}_{n_{\text{rep}}}(r_0)$	Outage probability in function of r_0 and n_{rep}
$\overline{\text{OP}}_{n_{\text{rep}}}$	Global outage probability averaged over r_0 or SF
$Th(n_{\text{rep}})$	Average effective throughput in function of n_{rep}
$\text{OPAloha}_{n_{\text{rep}}}(r_0)$	Outage probability in pure Aloha scenario in function of r_0 and n_{rep}
$\overline{\text{OPAloha}}_{n_{\text{rep}}}$	Global outage probability in pure Aloha scenario averaged over r_0 or SF
$ThAloha(n_{\text{rep}})$	Average effective throughput in function of n_{rep} in pure Aloha scenario
$\text{OP}_{n_{\text{rep}}}(SF)$	Outage probability in function of SF and n_{rep}
$Th_{SF}(n_{\text{rep}})$	Average effective throughput of a certain SF in function of n_{rep}

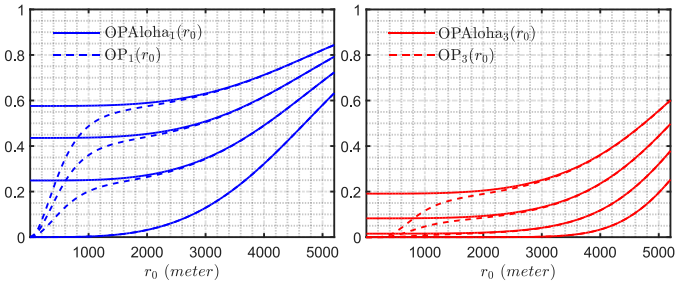

Fig. 3. Outage probability in function of r_0 and N. The solid line represents the pure Aloha case, the dashed line the case with capture effect. The five series of curves in each sub figure represent from top to bottom the case where $N = 30000, 20000, 10000, 1$.

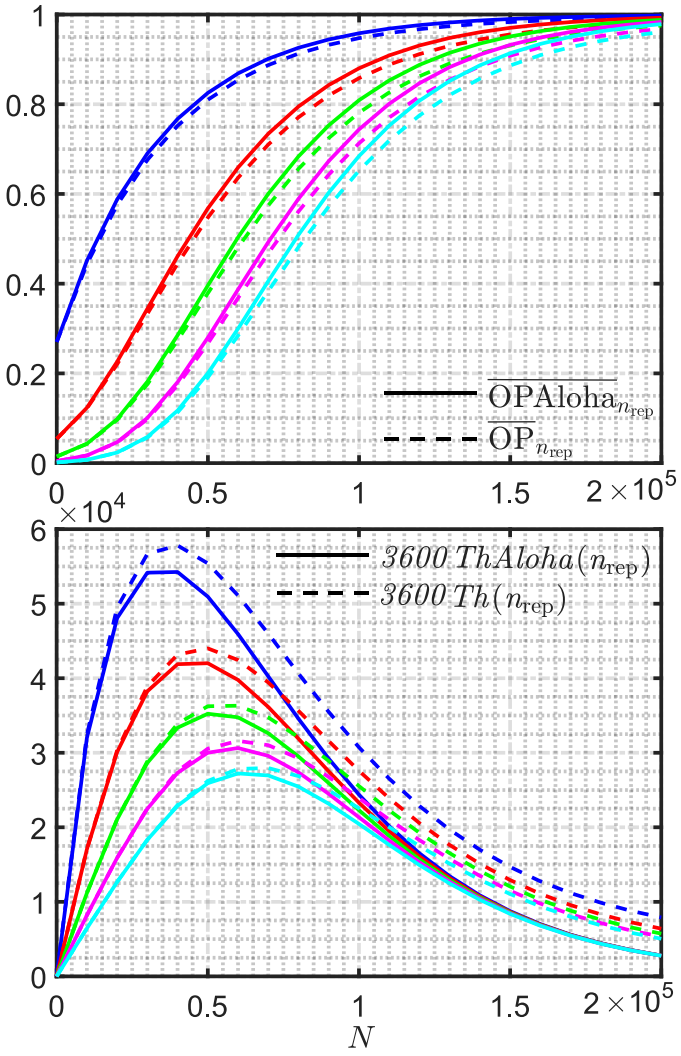

Fig. 4. Global outage probability and average effective throughput in one hour for Sigfox® scenario. The five colors in each sub figure from top to bottom represent $n_{\text{rep}} = 1, 3, 5, 7, 9$. Solid line represents the pure Aloha case, dashed line the case with capture effect.

redundancy. Our abacuses permits to find the optimal n_{rep} in function of the target outage probability, N, throughput and energy cost.

B. LoRaWAN®

1) 1D "cards tossing" parameters : LoRaWAN® is another LPWA technology based on spectrum spreading [22]. The spreading factor is denoted by SF and can vary from 6 to 12. Every packets are spread in the available bandwidth F, *i.e.*, $\Delta f = F$. In Europe 3 default channels are used, each with a bandwidth of 125kHz [22]. Different SF result in different bit rate. The smaller the SF, the higher the bit rate. Different payload sizes are also specified for different SF. Δt_{SF} can thus be calculated, the detail can be found in [13], [23]. T_{SF} is fixed to $100\Delta t_{SF}$ according to the ETSI duty cycle constraint of 1% [21] in the 868MHz band. Transmissions from different SF are considered orthogonal and do not interfere with each other [13], [16], [23], so the "cards tossing" game of LoRaWAN® can be seen as seven orthogonal and parallel 1D games described in section IV-A, each having three orthogonal channels of bandwidth $F = 125$kHz, different Δt_{SF} and T_{SF}. The corresponding game parameters are listed in table I and III [13], [23].

2) Multiple annuli cell structure: The greater the SF, the lower the sensitivity of transmission associated [23] . This results in smaller ζ_{SF} required for greater SF. Transmission with greater SF can thus reach further. r_{SF} is defined as the maximum distance that a transmission with a certain SF can barely reach, with only path loss considered, *i.e.*, $\frac{\rho_{tm} r_{SF}^{-\beta}}{\gamma} = \text{SNR} = \zeta_{SF}$, where $\rho_{tm}\Delta f$ takes the maxmimum allowed power 14dBm [21]. The noise power is around -117dBm. Let's add a shadow margin of 10 dB as well as a penetration loss of around 15 dB, to give us the ζ_{SF} for different SF, see table III. The path loss exponent n is fixed to the same 3.6 as in Sigfox® scenario. With the maximal allowed transmission power $\rho_t \Delta f$ of 14 dBm, the communication ranges r_{SF} in terms of path loss for different SF are thus calculated and listed in table III. These are the ranges with which the reception $\text{SNR} = \frac{\rho_t r_{SF}^{-n}}{\gamma}$ barely satisfies ζ_{SF}, in presence of only path loss and without considering fading and interferences, *i.e.*, $\zeta_{SF}^{-1} - \text{SNR}^{-1} = 0$.

Further devices should use greater SF to simply reach out to the base station, while nearer devices can benefit from higher bit rate of smaller SF. Let's consider a ideally pre-configured network where all the devices located in the annulus defined by r_{SF} and r_{SF-1} take spreading factor SF (For $SF\,6$, it's the annulus between r_6 and r_c) so that they make use of the smallest possible SF and thus the highest possible bit rate while guaranteeing the communication range at the same time [13], [15]. The probability of a node falling into a certain annulus denoted by p_{SF} is proportional to its surface [15]. The number of devices taking a certain SF is thus just Np_{SF}. ζ_{SF}, r_{SF} and p_{SF} are listed in table III.

LoRaWAN® network support over-the-air activation of the node which requires the node to open 2 successive downlink windows after a uplink transmission, in order to receive the MAC layer commands from the network [22]. Also, LoRaWAN® network infrastructure can manage the SF and date rate by means of an ADR (Adaptive Data Rate) scheme, which also necessitates the node to listen to gateway downlink transmissions. Note that the downlink and uplink in LoRaWAN® share the same channels, so collision phenomenon may be aggravated by the use of downlink. The pre-configured network that we consider is the scenario without nodes listening to gateway, *i.e.*, there is only uplink transmissions. Each node is set to an appropriate SF according to its distance from the gateway.

3) Outage and throughput model with power control scheme for LoRaWAN®: To improve the fairness of devices located in the same annulus and having the same SF, we consider the following ideal power allocation strategy : Allocate $\rho_{tm}\Delta f = 14$dBm to the devices with distance r_{SF} to make sure they get covered; Make sure that the reception power density attenuated by path loss of all devices in the same

TABLE III
PARAMETERS OF LORAWAN®

SF	Sensitivity (dBm)	ζ_{SF} (dB)	Range r_{SF}(km)	p_{SF}	Payload (bytes)	Δt_{SF} (s)	Bit rate (Kb/s)	T_S
6	-121	21	1.13	0.13	242	0.233	8.309	23.
7	-124	18	1.37	0.06	242	0.400	4.840	40.
8	-127	15	1.67	0.09	242	0.707	2.738	70.
9	-130	12	2.02	0.13	115	0.677	1.359	67.
10	-133	9	2.45	0.19	51	0.698	0.585	69.
11	-135	7	2.78	0.17	51	1.561	0.261	156.
12	-137	5	3.16	0.23	51	2.793	0.146	279

annulus, denoted by ρ, is identical and equal to that of devices with distance r_{SF}, *i.e.*, $\rho_{tm} r_{SF}^{-\beta}$. Fading effect is neglected in this case. This setting falls into the perfect power control paradigm introduced in sub section III-C2. $\zeta_{SF}^{-1} - \mathrm{SNR}^{-1} = 0$ according to the section V-B2. By shrinking all the annuli, our power allocation scheme can in fact result in non zero $\zeta_{SF}^{-1} - \mathrm{SNR}^{-1}$. With cdf of X_Σ already given in section IV, there is no problem in evaluating this adaptation.

In our scenario, the non fairness between devices with the same SF but different distance r_0 is removed, *i.e.*, $\mathrm{OP}_{n_{\mathrm{rep}}}$ doesn't depend on r_0 any more, but non fairness exists between different SF as SF with greater p_{SF} have greater device number Np_{SF} and thus greater $\mathrm{OP}_{n_{\mathrm{rep}}}(SF)$ expressed as $\mathrm{OP}_{n_{\mathrm{rep}}}(SF) = \left[\Pr\left[X_{\sum_{k=1}^{N_{SF}}} \geq 0\right]\right]^{n_{\mathrm{rep}}}$. $Th(n_{\mathrm{rep}}) = \sum_{SF=6}^{12} Th_{SF}(n_{\mathrm{rep}})$ should be recast as follows,

$$Th(n_{\mathrm{rep}}) = \sum_{SF=6}^{12} \frac{3Np_{SF}(1 - \mathrm{OP}_{n_{\mathrm{rep}}}(SF))}{T_{SF}\, n_{\mathrm{rep}}} \qquad (17)$$

where the factor three comes from the three available channels. The outage probability averaged over SF is expressed as $\overline{\mathrm{OP}}_{n_{\mathrm{rep}}} = \sum_{SF=6}^{12} \mathrm{OP}_{n_{\mathrm{rep}}}(SF) p_{SF}$. Quantities to be simulated are listed in table II. Note that in the scenario considered, $\overline{\mathrm{OP}}_{n_{\mathrm{rep}}}$ coincides with $\overline{\mathrm{OPAloha}}_{n_{\mathrm{rep}}}$, and $Th(n_{\mathrm{rep}})$ with $ThAloha(n_{\mathrm{rep}})$ as there is no tolerance of overlapping.

4) Simulation: The simulation results in the LoRaWAN® case are given in figures 5 and 6. Figure 5 shows the non fairness in terms of outage probability between different SF, which is directly related to p_{SF}, which again is dictated by non uniformity of device density in function with r_0.

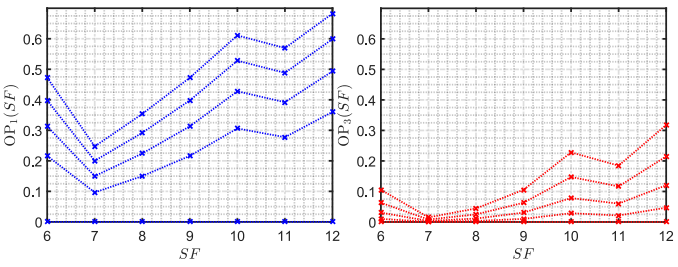

Fig. 5. Outage probability of LoRaWAN® in function of N and SF. From top to bottom, the five curves in each sub figure represent $N = 250, 200, 150, 100, 1$. Sub figure on the left is the case where $n_{\mathrm{rep}} = 1$, on the right $n_{\mathrm{rep}} = 3$.

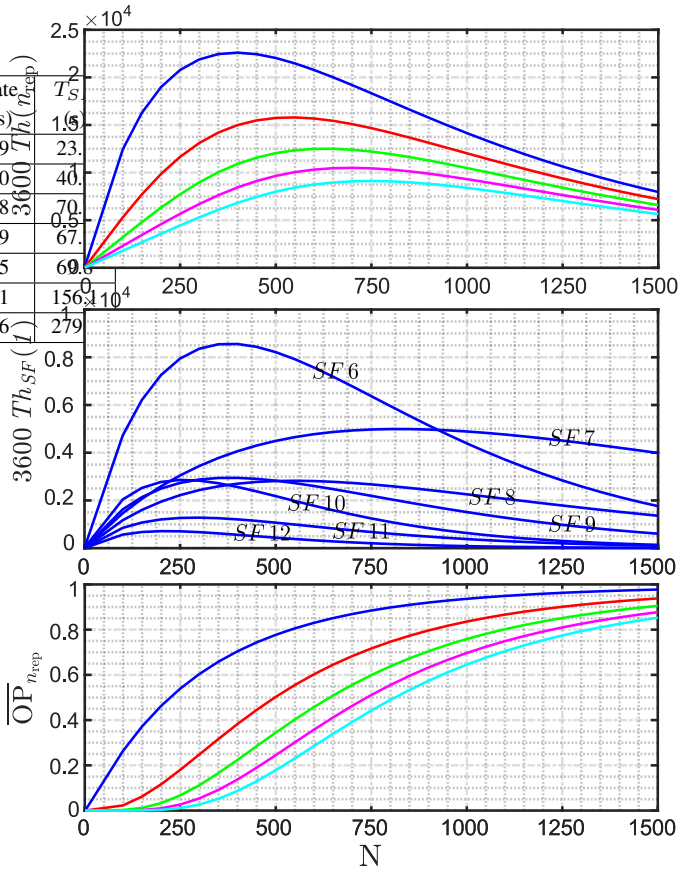

Fig. 6. The figure in the top represents average effective throughput in one hour. The five different colors from top to bottom represent the case $n_{\mathrm{rep}} = 1, 3, 5, 7, 9$. The figure in the middle represents average effective throughput in one hour of different SF, with $n_{\mathrm{rep}} = 1$. The numbers on the curves stand for the SF. The figure in the bottom represents the global outage probability. The colors have the same meaning as described earlier.

Several observations can be made from figure 6. First, repetition mechanism reduces overall outage probability but also the average effective throughput as redundancy is introduced. It increases energy cost as well. Second, the differences between $Th_{SF}(n_{\mathrm{rep}})$ are multiple, dictated by p_{SF} and T_{SF}. p_{SF} determines $OP_{n_{\mathrm{rep}}}(SF)$, while T_{SF} determines the speed of message sending. For example, $SF\,6$ is the fastest of all SF, but as $p_6 > p_7$, the curve of $SF\,6$ reaches its maximum much earlier than $SF\,7$, which limits its performance. $SF\,12$ has the worst performance as it has the longest T_{SF} and biggest p_{SF}, which again confirms that the devices at the cell edge are probably the bottleneck of the network performance.

At last, if we try to compare Sigfox® and LoRaWAN®, we can see that even though Sigfox® can support more devices but in terms of throughput, it's of the same order as LoRaWAN®. Note that the payload sizes in LoRaWAN® are much more important than that of Sigfox® (see table I and III). It seems that Sigfox® is more suitable for applications with a lot of devices having smaller traffic, while LoRaWAN® can support applications with more important traffic but less devices.

VI. Conclusion and perspectives

In this article, we provide a high-level flexible model whose interest is illustrated by the performance evaluation of two LPWA technologies. To the best of our knowledge, this is the first model which considers joint time-frequency interference. Note that our paradigm can be adapted to other systems to evaluate the relationship between number of devices, repetition times, outage probability, throughput and energy cost. Capture effect is also taken into account in our model so further questions such as how to amplify it intelligently can be investigated in the future. We believe that our model provides a useful dimensioning tool for the future IoT scenarios.

Our model can be completed in the mathematical level. First, when the hypotheses $T \gg \Delta t$ and $F \gg \Delta f$ are not satisfied, algorithmic approach seems to be more adapted due to the difficulty in the probability evaluation on the border area. Second, the proportion between Δt and Δf has an influence on the probability distributions of X_k and X_Σ, thus comes the question of the best strategy of proportioning the time duration and frequency occupancy of the information packet, in order to minimize the overlapping. At last, it's possible to formulate a more general problem of finding the best strategy to use a 2D time-frequency resource, always in terms of minimization of overlapping phenomenon. We have the options between orthogonal division of the frequency band, division into multiple partially overlapping bands (POC), and random FDMA if we go to the extreme.

In both the LPWANs scenarios considered, cell edge devices seem to be the bottleneck of the global network performance. A possible solution is the densification of the infrastructure, knowing that IoT devices can communicate with multiple base stations *i.e.*, multiple reception or macro-diversity. A study on the k-coverage of devices is given in [24]. By combining the k-coverage model for LPWANs and our "cards tossing" model, we can jointly design the infrastructure deployment and MAC layer of devices, in order to improve the network performance while limiting the cost.

References

[1] Marco Centenaro, Lorenzo Vangelista, Andrea Zanella, and Michele Zorzi. Long-range communications in unlicensed bands: The rising stars in the IoT and smart city scenarios. *arXiv preprint arXiv:1510.00620*, 2015.

[2] George Margelis, Robert Piechocki, Dritan Kaleshi, and Paul Thomas. Low throughput networks for the IoT: Lessons learned from industrial implementations. In *Internet of Things (WF-IoT), 2015 IEEE 2nd World Forum on*, pages 181–186. IEEE, 2015.

[3] Lorenzo Vangelista, Andrea Zanella, and Michele Zorzi. Long-range IoT technologies: The dawn of LoRa™. In *Future Access Enablers of Ubiquitous and Intelligent Infrastructures*, pages 51–58. Springer, 2015.

[4] N. Abramson. The ALOHANet – surfing for wireless data. *IEEE Comm. Magazine*, 47(12):21–25, 2009.

[5] A. S. Tanenbaum and D. J. Wetherall. *Computer Networks*. Prentice Hall, Boston, 5th edition, 2011.

[6] Christopher Ware, Joe Chicharo, and Tadeusz Wysocki. Modelling of capture behaviour in ieee 802.11 radio modems. In *IEEE Int. Conf. on Telecomm.*, 2001.

[7] JENSC Arnbak and Wim Van Blitterswijk. Capacity of slotted ALOHA in Rayleigh-fading channels. *IEEE Journal on Selected Areas in Comm.*, 5(2):261–269, 1987.

[8] Kyungwhoon Cheun and Sunyoung Kim. Joint delay-power capture in spread-spectrum packet radio networks. *IEEE Transactions on Comm.*, 46(4):450–453, 1998.

[9] Jeongkeun Lee, Wonho Kim, Sung-Ju Lee, Daehyung Jo, Jiho Ryu, Taekyoung Kwon, and Yanghee Choi. An experimental study on the capture effect in 802.11 a networks. In *Proceedings of the second ACM international workshop on Wireless network testbeds, experimental evaluation and characterization*, pages 19–26, 2007.

[10] Arunesh Mishra, Vivek Shrivastava, Suman Banerjee, and William Arbaugh. Partially overlapped channels not considered harmful. In *ACM SIGMETRICS Performance Evaluation Review*, volume 34, pages 63–74, 2006.

[11] Eduard Garcia Villegas, Elena Lopez-Aguilera, Rafael Vidal, and Josep Paradells. Effect of adjacent-channel interference in IEEE 802.11 WLANs. In *2007 2nd international conf. on cognitive radio oriented wireless networks and comm.*, pages 118–125. IEEE, 2007.

[12] Guoliang Xing, Mo Sha, Jun Huang, Gang Zhou, Xiaorui Wang, and Shucheng Liu. Multi-channel interference measurement and modeling in low-power wireless networks. In *Real-Time Systems Symposium, 2009, RTSS 2009. 30th IEEE*, pages 248–257. IEEE, 2009.

[13] Konstantin Mikhaylov, Juha Petäjäjärvi, and Tuomo Haenninen. Analysis of capacity and scalability of the LoRa Low Power Wide Area Network Technology. In *European Wireless 2016; 22th European Wireless Conference; Proceedings of*, pages 1–6. VDE VERLAG GmbH, 2016.

[14] Claire Goursaud and Yuqi Mo. Random unslotted time-frequency aloha: Theory and application to iot unb networks. In *Telecommunications (ICT), 2016 23rd International Conference on*, pages 1–5. IEEE, 2016.

[15] Ferran Adelantado, Xavier Vilajosana, Pere Tuset-Peiro, Borja Martinez, and Joan Melia. Understanding the limits of LoRaWAN. *arXiv preprint arXiv:1607.08011*, 2016.

[16] Brecht Reynders, Wannes Meert, and Sofie Pollin. Range and coexistence analysis of long range unlicensed communication. In *Telecommunications (ICT), 2016 23rd International Conference on*, pages 1–6. IEEE, 2016.

[17] Shancang Li, Li Da Xu, and Shanshan Zhao. The internet of things: a survey. *Information Systems Frontiers*, 17(2):243–259, 2015.

[18] Muhammad Aljuaid and Halim Yanikomeroglu. Investigating the gaussian convergence of the distribution of the aggregate interference power in large wireless networks. *IEEE Trans. On Vehicular Tech.*, 59(9):4418–4424, 2010.

[19] Minh-Tien Do, Claire Goursaud, and Jean-Marie Gorce. On the benefits of random fdma schemes in ultra narrow band networks. In *Modeling and Optimization in Mobile, Ad Hoc, and Wireless Networks (WiOpt), 2014 12th Int. Symposium on*, pages 672–677. IEEE, 2014.

[20] Claire Goursaud and Jean-Marie Gorce. Dedicated networks for IoT: PHY/MAC state of the art and challenges. *EAI endorsed transactions on Internet of Things*, 2015.

[21] ETSI. http://www.etsi.org/deliver/etsi_tr/103000_103099/103055/01.01.01_60/tr_103055v010101p.pdf. Accessed: 2016-10-24.

[22] LoRaWAN™ Specification. https://www.lora-alliance.org/portals/0/documents/whitepapers/LoRaWAN101.pdf. Accessed: 2016-10-24.

[23] LoRaWAN™ Tranceiver Specification. http://www.semtech.com/images/datasheet/sx1272.pdf. Accessed: 2016-10-24.

[24] Zhuocheng Li, Tuong-Bach Nguyen, Quentin Lampin, Isabelle Sivignon, and Steeve Zozor. Ensuring k-coverage in low-power wide area networks for internet of things. https://hal.archives-ouvertes.fr/hal-01353801.